Hindawi
International Journal of Antennas and Propagation
Volume 2023, Article ID 5169206, 14 pages
https://doi.org/10.1155/2023/5169206

Research Article

Combined Open-Slot and Monopole 8 × 8 High-Isolation Broadband MIMO Antenna System for Sub-6 GHz Terminals

Jie Guo,[1] **Shaoqing Zhang**,[2] **Chong-Zhi Han**,[1] **and Liang Zhang**[1]

[1]*School of Ocean Information Engineering, Jimei University, Xiamen 361021, China*
[2]*Aviation Key Laboratory of Science and Technology on Electromagnetic Environmental Effects, Shenyang Aircraft Design and Research Institute, Shenyang 110013, China*

Correspondence should be addressed to Chong-Zhi Han; chongzhi_han@foxmail.com and Liang Zhang; liangzhang@jmu.edu.cn

Received 2 October 2022; Revised 15 November 2022; Accepted 3 April 2023; Published 24 April 2023

Academic Editor: Angelo Liseno

In this article, an 8 × 8 MIMO antenna system with multidecoupling structures is proposed for the fifth-generation (5G) terminal applications. First, an antenna element consisting of an L-shaped open slot with dimensions of 5.6 × 5 mm^2 and two bent-L-shaped monopoles with dimensions of 12.7 × 6.1 mm^2 is introduced. Due to coupling feed technology, the initial open slot owns a wide bandwidth from 3.62 GHz to 4.82 GHz. For broadening the bandwidth of the initial antenna element, two bent-L-shaped monopoles are added to the open slot to adjust the input impedance. By optimizing the parameters of monopoles, the proposed antenna element has been finally determined and the bandwidth of the antenna element has been broadened (2.82 GHz to 5.23 GHz). Second, a dual antenna pair is constructed by placing the two antenna elements with an edge-to-edge distance of 27 mm in a mirror image placement; the 8 × 8 MIMO antenna system is brought about by symmetrically disposing four such antenna pairs with an edge-to-edge distance of 47 mm. Moreover, the isolation of two closely placed antenna elements is achieved by the parasitic strip-loading technique and defective ground techniques. Due to the decoupling techniques used in the 8 × 8 MIMO antenna system, the average isolation has been optimized from 13.2 dB to 21.9 dB and the total efficiency of each antenna element has been improved from a worst 20% to over 45%. Besides, the calculated mean efficiency gain is less than 1 dB, and the calculated envelop correlation coefficient (ECC) is lower than 0.01 for desired frequency bands. Furthermore, the proposed 8 × 8 MIMO antenna system has the measured broadband bandwidth from 3.28 GHz to 5.05 GHz (covering N77, N78, and N79 bands) and a compatible dimension for ultra-thin mobile phones. The simulated results of this work are all obtained from EM software CST STUDIO SUITE 2019. In general, the proposed 8 × 8 MIMO antenna system with a high-isolation property provides a hopeful solution to 5G ultra-thin mobile phones.

1. Introduction

As fifth-generation (5G) technologies have been widely used, the number of connections to 5G mobile terminals has also skyrocketed. Antennas intended for 5G, especially for sub-6 GHz band terminal applications, are therefore highly regarded. Since the most investigated sub-6 GHz bands are N77 (3.3–4.2 GHz), N78 (3.3–3.8 GHz), and N79 (4.4–5 GHz), research focus involves the development of wideband antennas covering these bands [1–4]. Another research hotspot of sub-6 GHz antennas concerns improving the throughput of 5G terminals, where multi-input multi-output (MIMO) technologies have proved to be promising candidates [5, 6]; eight and more MIMO antenna elements have been validated to form reliable mobile terminal antenna systems, while most of them may possess insufficient bandwidth performance [7–11]. To summarize, wideband MIMO antennas covering the whole sub-6 GHz bands are of high significance for 5G terminal applications, whereas reported ones in the literature mostly operate in part of the band [12–16].

To achieve wide bandwidth coverage, numerous techniques have been proposed recently to broaden the bandwidth of MIMO antenna systems [17–25], among which using parasitic strips, lumped elements, or coupling feed is some common means of attaining multiresonance modes to

broaden bandwidth. For instance, in [18], multiresonance modes are realized using parasitic strips, while in [12], a T-shaped stub, an inverted L-shaped stub, and a bent L-shaped stub are added to the antenna element to achieve resonance modes at different frequencies of interest, and they are joined and optimized to obtain the desired response within the required frequency band. In the meanwhile, a lumped element-loading technique is also frequently used to achieve multiresonance modes in terminal MIMO antenna systems; such as in [19], the L-slot antenna loaded with lumped elements produced new resonant modes at adjacent frequency and broadened the bandwidth. As opposed to the former techniques, some techniques emphasize combination of existed modes; such as in [21], an inverted F planar antenna is etched with a T-shaped slot, and when the antenna is excited, the PIFA structure operates not only in a PIFA mode but also in a loop antenna mode and an open-slot mode. In this condition, all the existing resonant modes are combined to broaden the overall antenna bandwidth. It is worth noting that the abovementioned approaches can be applied to the same MIMO antenna system simultaneously by ingenious combination. Such as in [22], coupling feed and lumped element-loading techniques are used all together to enhance the bandwidth.

In addition to the bandwidth performance, MIMO antenna systems intended for sub-6 GHz domains are also faced with the problem of interelement interference. To mitigate mutual coupling, various decoupling techniques have been investigated [26–38]. The most popular idea behind isolation enhancement may be using reflectors or metamaterial-based reflection planes [33–38], neutral line decouples [27], and decoupling elements [28]. However, these methods are mostly applicable to narrow-band decoupling schemes. More recently, several new methods for wideband decoupling have also been proposed [29–32]. In [13], a common-mode and differential-mode synthesis-based mode cancellation method is proposed. Another mode decoupling method is proposed in [30] by inserting a connecting line between two slot antennas, and the straightforward structure brings about the odd and even mode to counterbalance original strong mutual coupling. Moreover, a metamaterial photonic bandgap (MTM-PBG) periodic structure is used as a decoupling frame to improve the isolation between transmit-receive (T/R) of MIMO systems in [32]. However, in a more concise fashion, one can simply combine two or more decoupling structures that work in different frequency bands to jointly achieve wideband isolation, such as in [22]. The prerequisite is that these decoupling structures do not interfere with one another.

In this article, a wideband 8×8 MIMO antenna system with desirable isolation performance is designed and fabricated. It contains eight analogous elements, and each element consists of two formations, that is, an open-slot fed by a coupling strip and two monopole branches fed by a microstrip line. Within each element, it uses L-shaped feeding branches to stimulate the open slot, thus achieving a relatively wide bandwidth. It also constructed two L-shaped folded monopoles on the sideboard, adjusting the overall input impedance of the antenna element to further broaden the bandwidth. Each element of the antenna system effectively covers N77, N78, and N79 bands (3.28 GHz–5.05 GHz). To mitigate mutual coupling, a T-shaped slot decoupling structure and a quasi-M slot structure with symmetric L-shaped parasitic strips are developed. With the decoupling structure of the antenna system, the measured isolation of arbitrary two ports of the antenna system is better than 14.5 dB over the operation bands. Based on the wideband technique and decoupling techniques, it readily fulfills an 8×8 MIMO antenna system by arranging eight sets of such antenna elements and six sets of such decoupling structures. Both simulated and measured results demonstrate that the 8×8 MIMO system possesses good isolation and diversity performance with isolation degrees better than 14.5 dB and ECCs lower than 0.01 across 3.28–5.05 GHz. The proposed 8×8 MIMO antenna system has wider bandwidth coverage than that of some recently proposed broadband terminal antennas [39–41], and it may be one of the attractive choices for 5G compact smartphone antenna system architects.

2. Design of the Antenna Element

2.1. Configuration. The configuration of the 8×8 MIMO antenna system as well as the design procedure is depicted in Figure 1. The antenna system consists of three pieces of printed circuit boards and eight radiating elements, as shown in Figure 1(a). The primary board (board $^{\#}1$ in the xy plane) has a dimension of 140 mm × 70 mm × 0.8 mm, while the two lateral boards (board $^{\#}2$ and board $^{\#}3$ in the yz plane) are placed perpendicularly to board $^{\#}1$ with a dimension of 140 mm × 8.6 mm × 0.8 mm. All the boards are fabricated with 0.8 mm-thick FR-4 material (with $\varepsilon_r = 4.4$ and loss tangent = 0.02).

Structures and detailed parameters of the antenna element are shown in Figures 1(b)–1(d). Each antenna element consists of two L-shaped folded monopoles printed on a lateral board (as shown in Figure 1(b)), feed structures printed on the primary board (as shown in Figure 1(c)), and an open slot etched also on the primary board (as shown in Figure 1(d)). For clarity, Figure 1(b) shows detailed dimensions of two L-shaped bent monopoles in the red and black dashed boxes, respectively. Figure 1(d) shows the detailed dimension of the L-shaped open slot. The feeding network for the element is shown in Figure 1(c). An L-shaped coupled brunch (denoted by a white dashed box in Figure 1(c)) is used to stimulate the open slot. Besides, the L-shaped bent monopoles are stimulated by a microstrip line with an L-shaped matching network (denoted by a purple dashed box in Figure 1(c)). Each antenna element is fed with a 50 Ω SMA connector through a via hole from the back side of board $^{\#}1$. Specifically speaking, we first designed an open-slot antenna with L-shaped coupling branches, as shown in Figure 1(e). The open slot's coupling feeding structure consists of a vertical microstrip line and an L-shaped coupling branch. To further broaden the bandwidth, we added two L-shaped monopoles to the antenna element. In addition, L-shaped monopoles are fed by lengthened microstrip lines, as shown in Figure 1(h). Due to the lengthening of

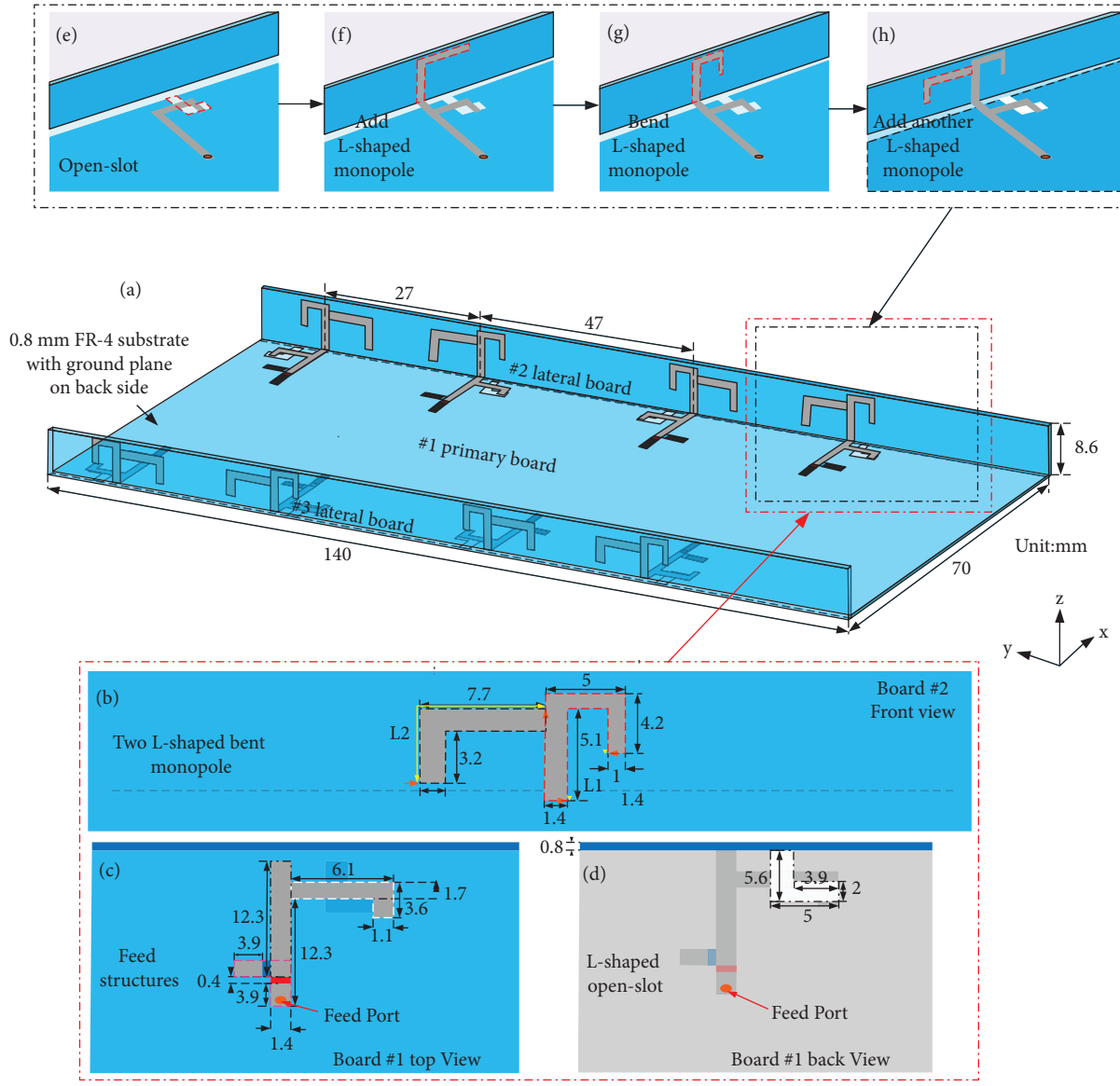

Figure 1: Configuration and design procedure of the antenna system.

the microstrip line, the feeding network of the open slot has changed. To modulate the input impedance, an L-shaped matching network (denoted by a purple dashed box in Figure 1(c)) is added to the feeding port.

2.2. Design Process and Analysis. As is well known, coupled-fed open-slot antenna has multiple resonant modes to produce broadband characteristics. Use of open-slot antenna elements to form wideband MIMO antenna systems has been well reported thereafter [42–45]. This work used L-shaped feed branches to stimulate open-slot antennas. To widen the bandwidth of the slot antenna without changing the slot size, two L-shaped folded monopoles are designed on the lateral board to adjust the overall impedance matching of the antenna element. It is satisfying that the branches did not impact the original resonant mode of the open-slot antenna. To illustrate the evolution process of the antenna element and the influence of the L-shaped monopoles on the impedance matching of the antenna element, we simulated the S-parameters and Z-parameters of the four evolved structures shown in Figures 1(e)–1(h).

The evolved structures are shown in Figures 1(e)–1(h). In Figure 1(e), we design an L-shaped open-slot structure and stimulate it with a coupling feed brunch. The simulated results are shown in Figure 2 case e, where the bandwidth of the open slot is 3.62 GHz to 4.82 GHz. To broaden the bandwidth, in Figure 1(f), we add an L-shaped folded monopole on the lateral board. This is inspired by [15] that different radiation structures may be combined altogether to improve the total bandwidth. Actually, by adding the L-shaped monopole, the bandwidth of the antenna element is significantly enlarged to 3.51–5.12 GHz.

To reduce the overall size of the antenna system, we fold the L-shaped monopole in Figure 1(g), and the antenna

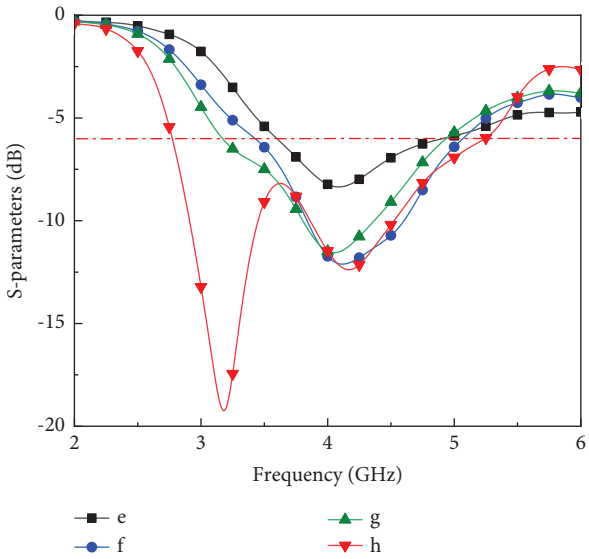

Figure 2: S-parameters of cases e–h.

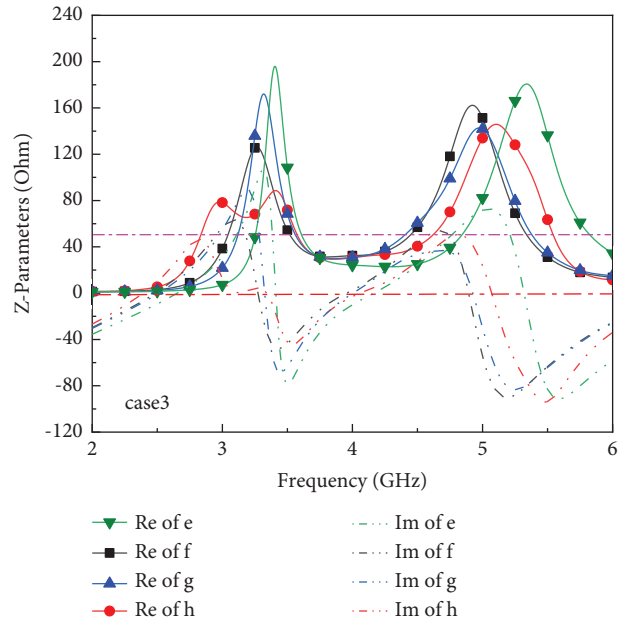

Figure 3: Z-parameters of cases e–h.

element bandwidth is shifted to 3.21–4.91 GHz. In Figure 1(h), another L-shaped folded monopole is disposed on the opposite side of the open slot. Adding this folded monopole caused the antenna element to be well-matched at 3 GHz and 3.3 GHz resonant modes, and the bandwidth is further extended to 2.8–5.2 GHz. It is intriguing to clarify how the folded L-shaped monopoles adjust the overall impedance matching of the antenna element. For this purpose, we simulate the Z-parameters for element structures of Figures 1(e)–1(h); the results are shown in Figure 3.

According to the simulated Z-parameters shown in Figure 3 case e, there are three resonances in the open-slot antenna. They are a monopole mode working at 3.3 GHz, a lower order mode of the open slot working at 4.2 GHz, and a higher order mode of the open slot working at 5.4 GHz, respectively. Only the real part of the lower order mode of the open slot at 4.2 GHz is close to 50 ohms in the three resonant states, and the other two resonant modes are mismatched. For Figure 3 cases f and g, owing to the L-shaped monopole, the matching of the higher order mode of the open-slot impedances at 5.4 GHz is adjusted, and the real part of the higher order mode of the open-slot impedances at 5.4 GHz is drawn from 200 ohms to almost 100 ohms, matching the 50-ohm input impedance better. Compared with case g, the other L-shaped bent monopole is added in Figure 3 case h. Obviously, the lower order mode of the open slot at 3 GHz is generated near the original one at 3.3 GHz. The real part of the input impedance from 3 GHz to 3.3 GHz is adjusted to be within 100 ohms. As the return loss demonstrated in Figure 2, the bandwidth of the proposed antenna element in Figure 1(h) is broadened to 2.82 GHz to 5.23 GHz. It covers the N77, N78, and N79 bands in the range of 3.3 GHz to 5 GHz.

To further optimize the antenna element, it is necessary to investigate the effect of the proposed monopoles on the broadband performance sufficiently. We simulated the S-parameters of two L-shaped folded monopoles with a total length of L_1 and L_2, respectively. As shown in Figure 1(b), the parameters of L_1 and L_2 are indicated by the solid yellow line segments. Figure 4(a) demonstrates the effect of L_1 values on S_{11} (note that L_2 is absent in this phase). With an increase in L_1 values, the bandwidth of the antenna element is broadened and extended toward the lower frequency range, while the performance in a higher frequency is affected at the same time.

Another L-shaped monopole branch is then added and swept. Figure 4(b) demonstrates the effect of different L_2 values on S_{11} (note that L_1 is fixed at an optimized value of 14.7 mm in this phase); with an increase in L_2 values, the S_{11} performance at higher frequencies are almost unaffected. Therefore, we adjusted L_1 and L_2 to jointly extend the working bandwidth. To ensure the working bandwidth to completely cover NR bands N77, N78, and N79 (3.3 GHz–5 GHz), we optimized $L_1 = 14.7$ mm and $L_2 = 17.4$ mm as the overall length of the two L-shaped folded monopoles, respectively. By optimizing such parameters, the final shape of the evolved antenna element is determined as in Figure 1(h).

3. Design of the MIMO System

The wideband performance of the proposed antenna element has been effectively verified in the above section. An 8×8 MIMO antenna system can be then designed for the terminal application. It is necessary to determine the position of the spatial arrangement of the antenna element. As shown in Figure 5, a pair of antenna elements can be arranged separately either in a parallel way (as Figure 5(a)) or in a mirrored way (as Figure 5(b)) on one certain side of the entire terminal structure. Figure 6(a) shows the simulation results of these two types of arrangement. When the two antenna elements are arranged in a mirror image, the bandwidth of the antenna element stimulated by port1 is

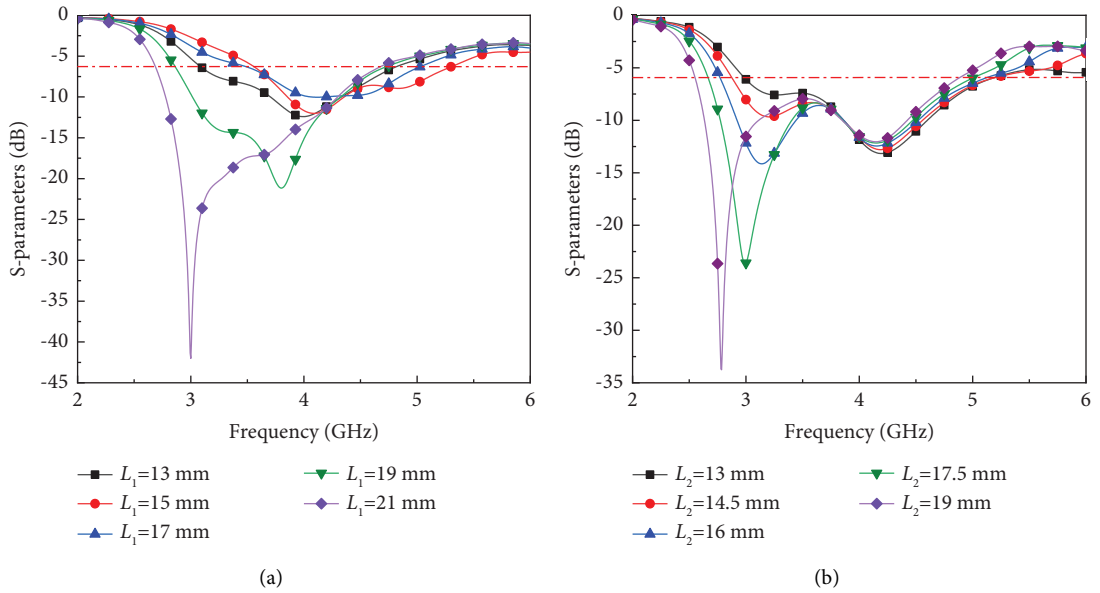

Figure 4: Simulated S-parameters (S_{11}) with different values of (a) L_1 and (b) L_2.

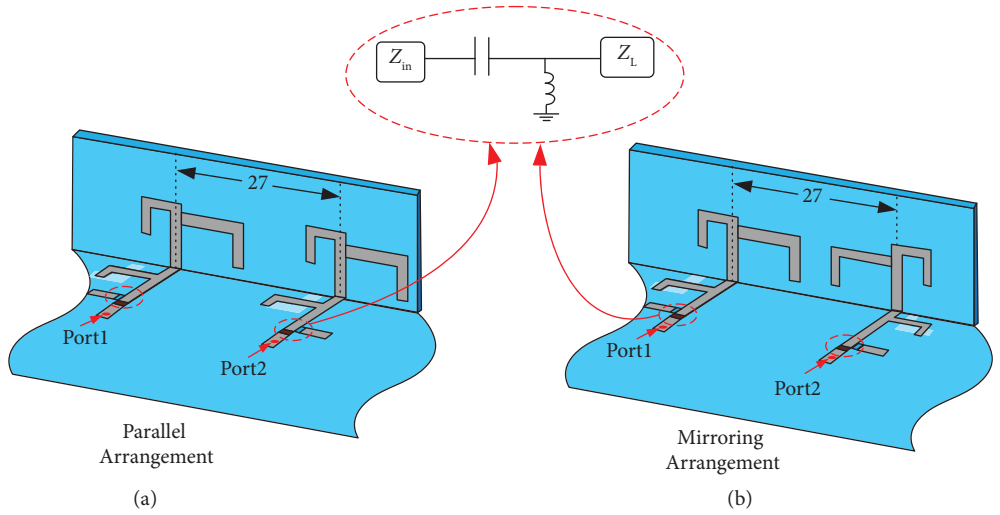

Figure 5: Arrangement of antenna elements: (a) parallel arrangement; (b) mirroring arrangement.

2.91–5.3 GHz, while the bandwidth stimulated by port2 is 2.82–5.1 GHz. The isolation degree between the two antenna ports is maintained above 12 dB. When the antenna elements are placed in a parallel way, the isolation of two ports at 2.8–3.3 GHz is kept at around 10 dB. Because of the lower isolation degree, S_{11} of the parallel-arranged antenna elements will be affected. As shown in Figure 6(b), S_{11} of paralleled components at 3.21–3.3 GHz cannot meet the requirement of lower than −6 dB. As a result, we decided to place the antenna elements in mirror images to attain better isolation performance.

Figure 7 shows an 8 × 8 MIMO antenna system consisting of four basic mirror images of antenna pairs arranged symmetrically. Owing to the symmetric deployment of the antenna pairs, only the S-parameters from port1 to port4 need to be simulated. According to the results presented in Figure 7, the working bandwidth meets the coverage demand of N77, N78, and N79 (3.3 GHz–5 GHz). However, the isolation degree between port2 and port3 is less than 10 dB between 2.81 GHz and 3.62 GHz, and the isolation degree between port1 port2, port3, and port4 lies within the range of 10 dB to 15 dB over the frequency range of 3.62 GHz to 5.12 GHz. The isolation degrees between other ports are all above 15 dB. Due to the deterioration of isolation from port2 to port3 over 2.81 GHz to 3.62 GHz, decoupling structures are quite necessary for this antenna system.

The following text describes how to design the decoupling structures for the proposed 8 × 8 system.

First, the key positions of interelement coupling should be determined; then, appropriate decoupling structures should be chosen. We take three observation points in the operating bands of 3.3 GHz, 4.1 GHz, and 5 GHz to

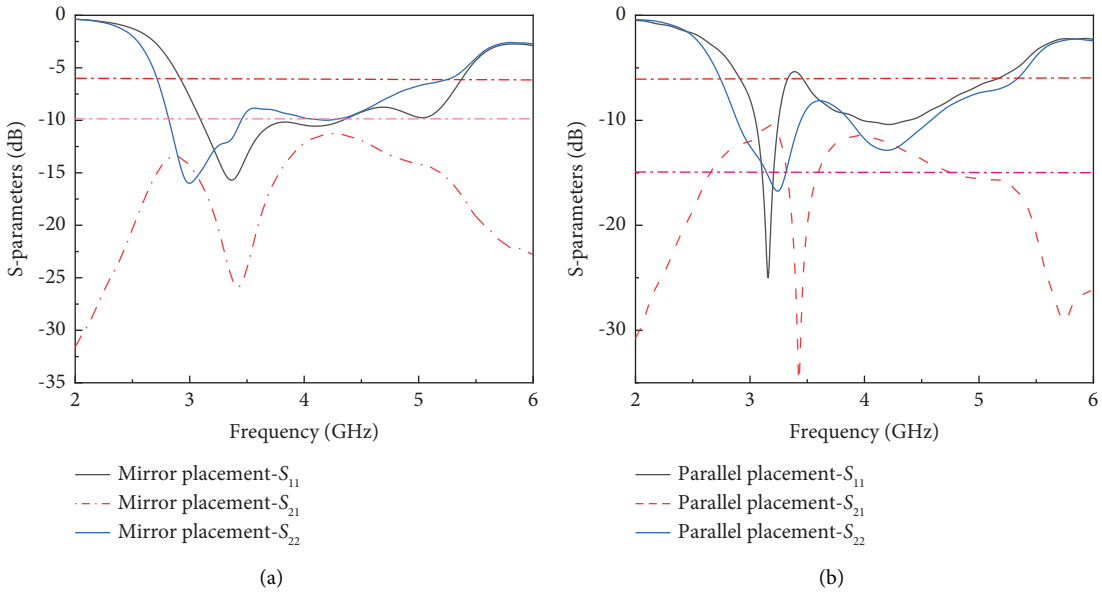

Figure 6: Simulated S-parameters with different arrangements: (a) S-parameters of two-element antennas in parallel arrangement; (b) S-parameters of two-element antennas in mirror arrangement.

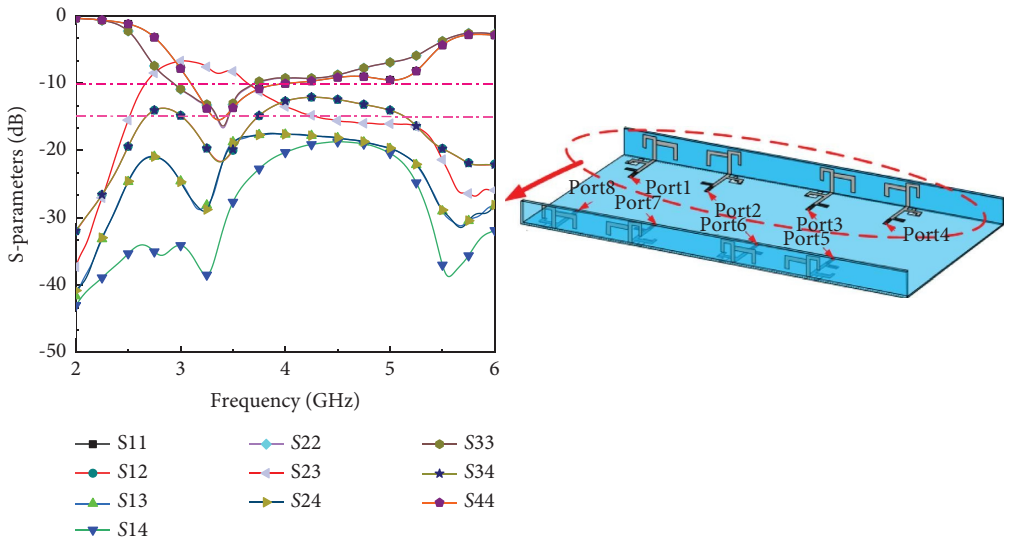

Figure 7: Geometry and S-parameter simulation of a centrosymmetric 8 × 8 MIMO antenna system.

investigate the occurrence of coupling. Current distributions between port1 and port2 without decoupling structures are shown in the Figure 8(a) left panel (marked red), where surface current stimulated by port1 is directly coupled into port2. Inevitably, the radiation from one element will be partly coupled into the other element. Note that the L-shaped monopoles as well as the open slot will be stimulated by strong coupling, and therefore, it is necessary to develop decoupling structures between port1 and port2 to maintain performance of each element. As for port2 and port3 (coupling between two pairs), current distribution between the pairs without decoupling structures is shown on the left panel (marked red) of Figure 8(b). For instance, when the radiation structure is stimulated by port2 at 3.3 GHz, it causes a large amount of coupling current to pour into port3. The isolation degree between port2 and port3 at 3.3 GHz is less than 10 dB, as indicated by simulated S_{23} in Figure 7. Thus, decoupling structures are also needed between the four pairs.

According to the current distribution shown in Figures 8(a) and 8(b), the coupled currents around the L-shaped open-slot radiation structures are dense in all conditions. To suppress coupling currents, we designed the decoupling structures for L-shaped slots first. Figure 9 case 1 first introduces a slot in the ground between port1 and port2; the isolation degree of both the ports is directly increased from 10 dB to more than 15 dB, as shown in Figure 10(a), which verifies the effectiveness of the slot defective ground

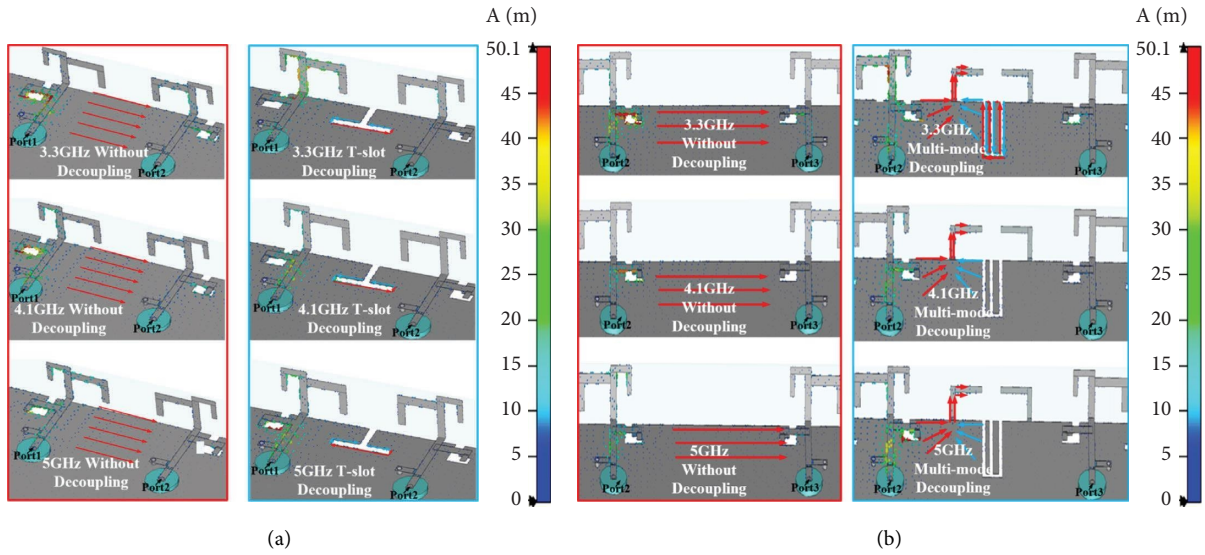

FIGURE 8: Current distribution in the vicinity of two ports with or without: (a) T-slot decoupling structures and (b) quasi-M slot combining parasitic strips decoupling structures.

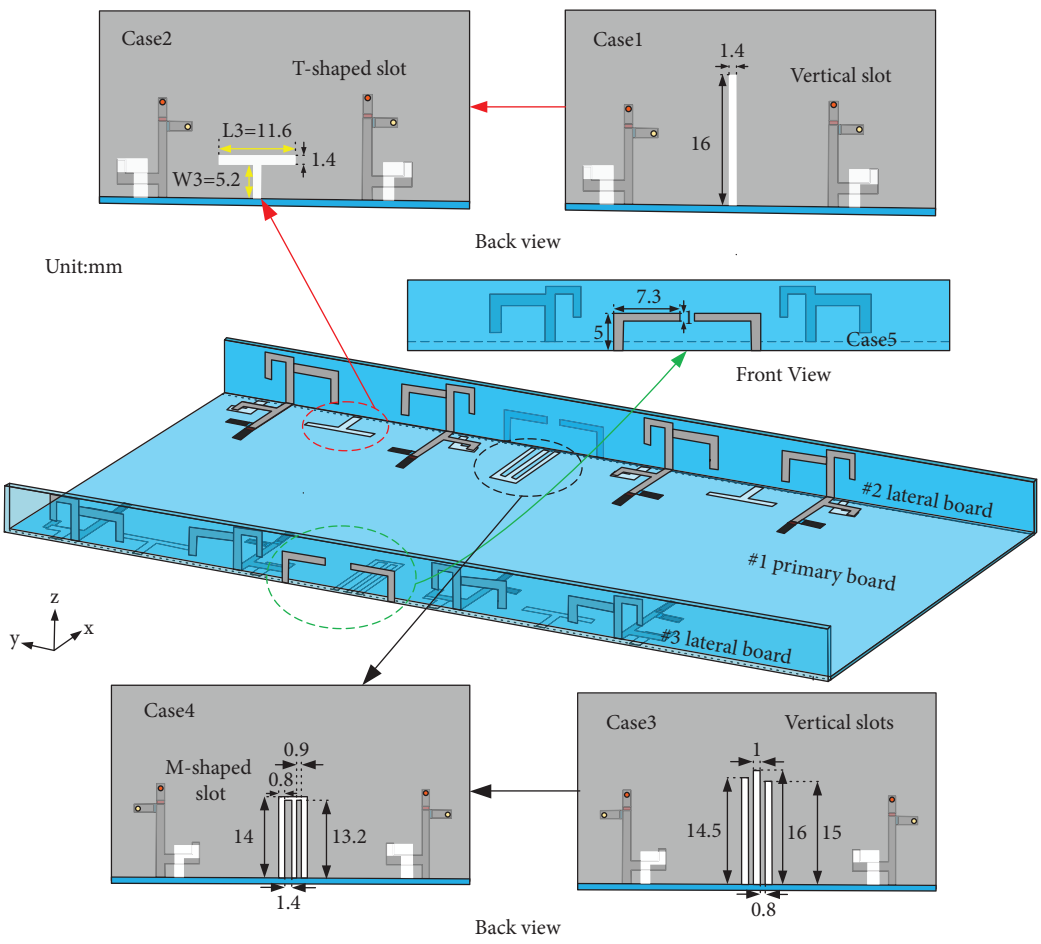

FIGURE 9: Design and detailed dimensions of the proposed decoupling structures.

structure. However, concerning the long slot length, we substituted it with a T-shaped slot. A T-shaped slot is etched on the ground between port1 and port2 in Figure 9 case 2. The length and width of the T-shaped slot are set as L_3 and W_3, respectively (denoted by yellow bidirectional arrows). The W_3 value is set close to the width of the radiating open slot, which

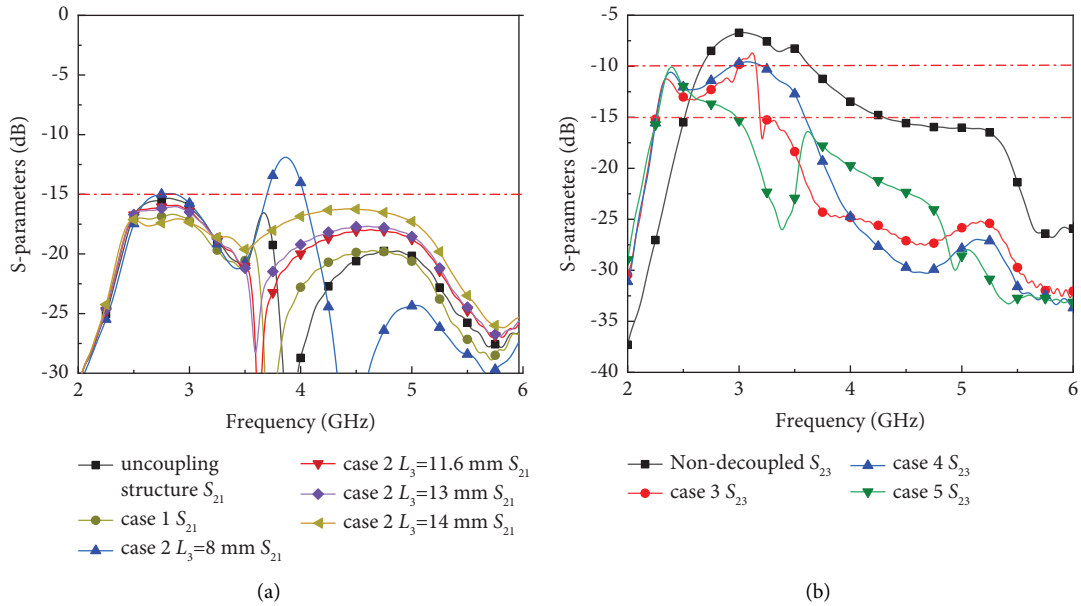

Figure 10: Decoupling structure evolution process.

is $W_3 = 5.4$ mm. A parameter sweep for L_3 was conducted to fathom the effect of the horizontal length of the T-shaped slot on isolation performance between port1 and port2. In Figure 10(a) case 2, an optimal isolation degree of over 18 dB is achieved for N77, N78, and N79 (3.3 GHz–5 GHz) when $L_3 = 11.6$ mm.

As shown in the Figure 8(b) left panel (marked red), the current coupling from port2 to port3 is mainly propagated through the ground plane. Therefore, suppressing the coupling currents of the ground plane is the most effective means to get high isolation. Since the ground plane's vertical slot can typically suppress coupling currents by cutting horizontal currents and suppressing vertical currents, the vertical slot is used in our work. However, single vertical slot typically has a long vertical dimension and is just suitable for narrow-band decoupling situations. Since the coupling strength between two pairs (e.g., port2 to port3) is much greater, we designed multiple slot structures, as shown in Figure 9 case 3. Simulated S_{23} of case 3 is shown in Figure 10(b), and these multiple slot decoupling structures improved the isolation degree between port2 and port3 from the worst case of less than 7 dB to greater than 10 dB. Similarly, it is necessary to further optimize the size of these vertical slots. We proposed a slot decoupling structure of quasi-M shape (refer to Figure 9 case 4) and a pair of L-shaped symmetric parasitic strips (refer to Figure 9 case 5). The L-shaped symmetric parasitic strips are placed on the outside of the lateral boards. According to Figure 10(b), the isolation degree between port2 and port3 is increased from 10 dB to 14.5 dB.

To validate the effectiveness of the decoupling structures, the current distribution at three frequencies of 3.3 GHz, 4.1 GHz, and 5 GHz for antenna elements with the above decoupling designs is illustrated in Figure 8(a) and 8(b) right panels (marked blue). The phase of currents along the T-shaped decoupling structure is opposite, as is shown in blue and red arrows, respectively, in which sense the currents cancel out one another, and therefore, the far-field radiation from the coupled current is weakened. As the comparison with and without decoupling structures indicated, the current intensity near port2 is significantly reduced by decoupling techniques. Moreover, the current intensity near the radiating structure of port2 antenna elements also decreases. Second, opposite-phase currents of the quasi-M slot at 3.3 GHz are also marked by the blue and red arrows in the Figure 8(b) right panel. Like the T-shaped slot, the quasi-M slot produces decoupling characteristics by cancelling out the opposite-phase coupling current radiation in the far field. Last but not least, the opposite-phase currents (denoted by blue and red arrows) near the L-shaped parasitic strips are shown in Figure 8(b). L-shaped parasitic strips changed the phase of coupled current in the primary board; thus, the coupling from port2 to port3 is suppressed. Since the antenna system is symmetric, the same decoupling method can be reused between the symmetry ports. Hence, the overall isolation of the proposed wideband 8×8 MIMO antenna system is guaranteed.

Table 1 compares the proposed wideband 8×8 MIMO antenna system with existing ones in the literature. First, the antenna element proposed in this paper has significant advantages in the bandwidth coverage range. The referenced antennas listed in Table 1 typically have bandwidth coverage within 1 GHz [13–15, 23, 24, 43, 45]. In addition, the operating band of these antennas is mostly in noncontinuous frequency ranges [12–15, 25, 44]. Second, the isolation degree of the proposed antenna is more than 14.5 dB. Although 14.5 dB is not the highest in Table 1, the high isolation of the proposed antenna is achieved in the broadband range (3.28–5.05 GHz), which is a nontrivial task. Furthermore, compared with [43–45], the proposed antenna element has a smaller horizontal dimension, in condition that the vertical

Table 1: Comparison of the proposed antennas with other works for 5G smartphones.

Ref.	Size (mm × mm)	Bandwidth (GHz)	Efficiency	ECC	Isolation (dB)	Numbers
[11]	3 × 15	2.4–3.6	40%–60%	<0.15	>13	8 × 8
[12]	5.77 × 18	3.1–3.6/4.4–6.1	50%–75%	<0.1	>18.5	8 × 8
[13]	4 × 8	3.4–3.6/5.1–5.7	58%–74%	<0.02	>14	8 × 8
[14]	3 × 14	3.34–3.7/4.67–5.08	55%–72%	<0.08	>12	8 × 8
[15]	4.2 × 9	3.38–3.82/4.75–5.13	60%–75%	<0.008	>14.5	8 × 8
[23]	14.5 × 12	3.21–3.81	90%–95%	<0.02	>10	4 × 4
[24]	12.5 × 18.5	3.4–3.6	42%–65%	<0.2	>12	8 × 8
[25]	2.5 × 18	3.1–3.9/5.5–6.3	70%–80%	<0.035	>12	8 × 8
[43]	9.5 × 3	3.4–3.6	62%–84%	<0.1	>14.8	8 × 8
[44]	3 × 19.3	3.4–3.8/5.15–5.925	83%–93%	<0.06	>20	10 × 10
[45]	10 × 3.5	3.3–3.8	87%–93%	<0.01	>16	18 × 18
This work	5.6 × 5/12.7 × 6.1	3.28–5.05	45%–82%	<0.01	>14.5	8 × 8

dimensions of the proposed antenna elements meet the required limits of the terminal and that more such antenna elements with smaller horizontal dimensions can be accommodated in the same terminal; this is obviously conducive to integration. In summary, compared with the existing work, this antenna has significant advantages in wide bandwidth, high-isolation broadband degrees, and small horizontal dimensions. Thus, the proposed 8 × 8 MIMO antenna system provides a hopeful solution to 5G ultra-thin mobile phones.

A prototype was fabricated to demonstrate the feasibility of the proposed 8 × 8 MIMO antenna system (shown in Figure 11(a)). Since the structure is symmetric, only the reflection coefficients of port1, port2, port3, and port4 are shown for brevity. Both simulated and measured reflection coefficients are better than −6 dB across the desired N77, N78, and N79 bands (from 3.28 to 5.05 GHz, as shown in Figure 11(b). The slight difference in the reflection coefficients between antenna element 2 and element 3 is attributed to the quasi-M decoupling slot, and it is not a perfectly symmetric M-shaped structure and therefore causes disagreement. The measured result of the isolation degree between different antenna elements is shown in Figure 11(c). A slight frequency shift occurred between the simulated and measured results, due to the fabrication process of PCB and instability of the FR-4 dielectric constant. The isolation of any two ports in the range of 3.3 GHz to 5 GHz is above 14.5 dB. A good agreement is observed between simulation and measurement. The total efficiency of the antennas is also measured, as shown in Figure 11(d). In the range of the 5G-NR bands, the measured total efficiency of ANT1 and ANT4 antenna elements is 59% to 79%, and the total efficiency of ANT2 and ANT3 antenna elements is 45% to 82%. For the reason of symmetry, we display the simulated and measured ECCs of every two antennas from ANT1 to ANT4 (as shown in Figure 11(e)). Within the range of the 5G-NR bands, the measured ECC between each two ports is less than 0.01. In this paper, all ECC values of the proposed antenna system are obtained based on radiation patterns:

$$\mathrm{ECC} = \frac{\left|\iint_{4\pi} G_i(\theta,\phi)\, G_j(\theta,\phi) * \partial\Omega\right|^2}{\iint_{4\pi}\left|G_i(\theta,\phi)\right|^2 \partial\Omega \iint_{4\pi}\left|G_j(\theta,\phi)\right|^2 \partial\Omega}\ \#. \quad (1)$$

Finally, the 3D radiation pattern of the antenna is simulated and measured at 3.3 GHz, 4.1 GHz, and 5 GHz, which is shown in Figure 12.

Figure 13(a) depicts the diversity gain of the proposed MIMO antenna system, and it is observed that the diversity gain fluctuates around a 10 dB scale for the entire operating band (3.3 GHz to 5 GHz). The mean efficiency gain (MEG) indicates the gain of the system in a multipath environment. The calculated MEG is less than 1 dB for desired frequency bands, as shown in Figure 13(b). In addition, the channel capacity of the proposed MIMO antenna system is calculated by averaging the Rayleigh fading realization with a referenced signal-to-noise ratio (SNR) of 20 dB. The peak channel capacity is found to be 35.2 bps/Hz, as illustrated in Figure 13(c).

Moreover, the proposed 8 × 8 MIMO antenna grabbed by a single hand and double hand is set up and simulated. As shown in Figure 14(a), an LCD screen ($140 \times 70\ \mathrm{mm}^2$ large, with $\varepsilon_r = 4.82$, and loss tangent = 0.0054) is installed on the top of the antenna's terminal panel, and a battery with a dimension of $94 \times 23\ \mathrm{mm}^2$ is also installed at the center of the antenna's terminal panel. The battery uses two-layer structures: the upper layer is made of material named "battery_shell" (with $\varepsilon_r = 1.5$ and loss tangent = 0.02), and the bottom layer is made of copper. For both regions of a single hand and double hand, the simulated reflection coefficients of all the antenna elements are better than −6 dB across the desired N77, N78, and N79 bands (from 3.25 to 5.03 GHz, as shown in Figure 14(b). For the isolation degree in the region of the human hands, the isolation degree between the antenna elements in both the single-hand region and double-hand region is greater than 14.5 dB, as shown in Figure 14(c). However, the total efficiency of the antenna elements in the human hand area is degraded, as shown in Figure 14(d). In the case of single-handed operation, the reduction in radiation efficiency is noted for ANT5 and ANT8, whereas for the double-hand scenario, ANT2 and ANT3 provide less radiation efficiency. This is due to the features of human body tissue (fingers near the antenna), which absorb a lot of antenna radiation power. On the whole, the proposed MIMO antenna system offers radiation efficiencies in the range of 35–75% for both scenarios for the desired frequency band.

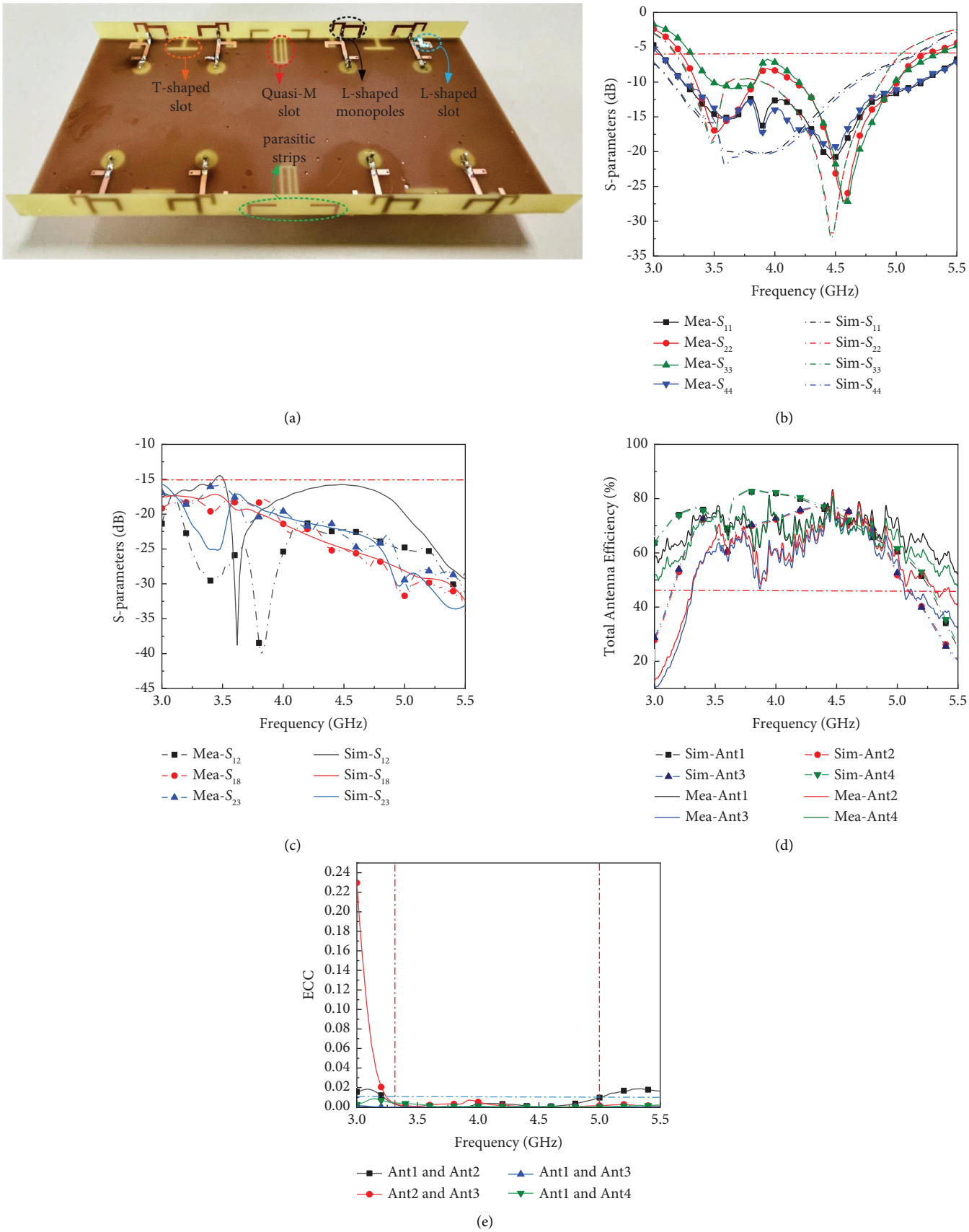

FIGURE 11: Prototype and measurement: (a) prototype of the proposed antenna system; (b) *S*-parameter simulation and measurement of the proposed antenna system; (c) isolation simulation and measurement of the proposed antenna system; (d) total efficiency simulation and measurement of the proposed antenna system; (e) calculated ECC of the proposed antenna system.

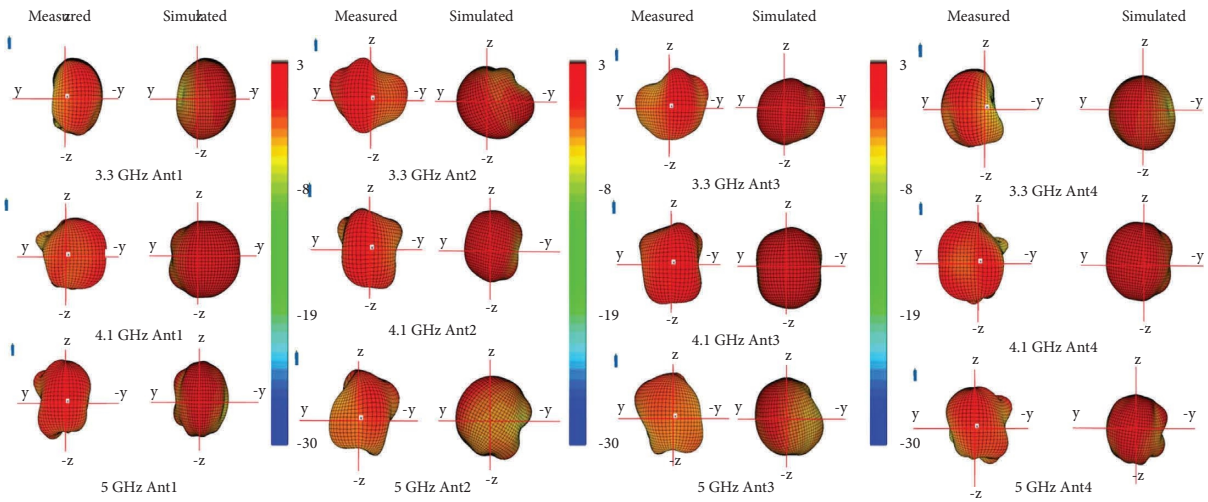

Figure 12: 3D radiation pattern of ANT1–ANT4.

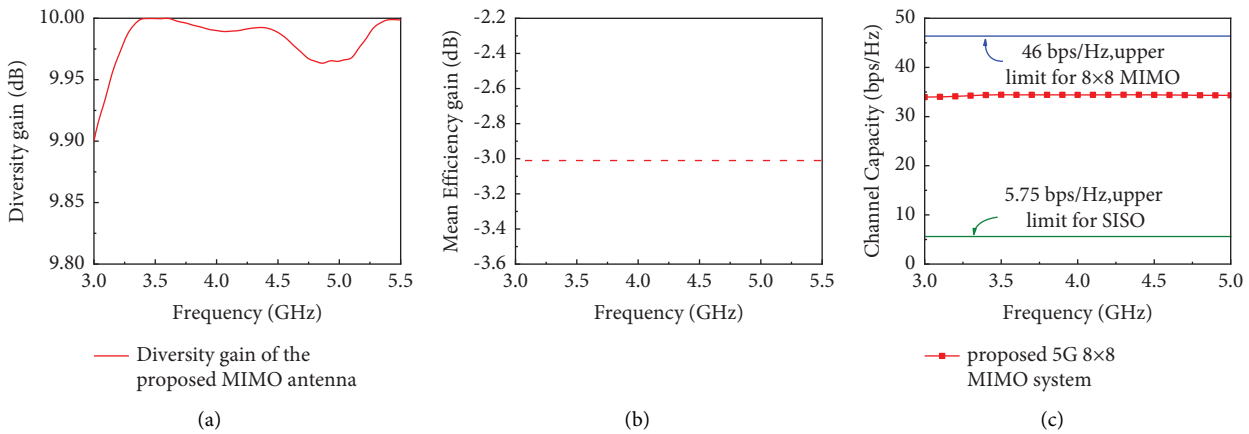

Figure 13: Performance of the proposed antenna system: (a) diversity gain; (b) mean efficiency gain; (c) channel capacity.

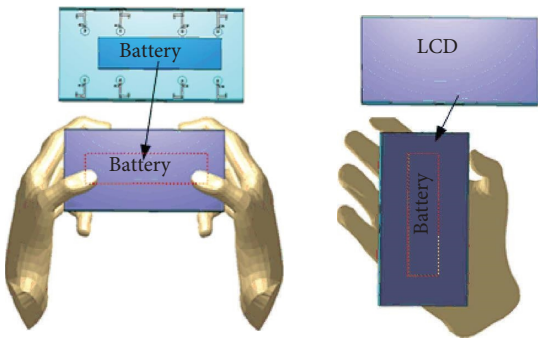

(a)

Figure 14: Continued.

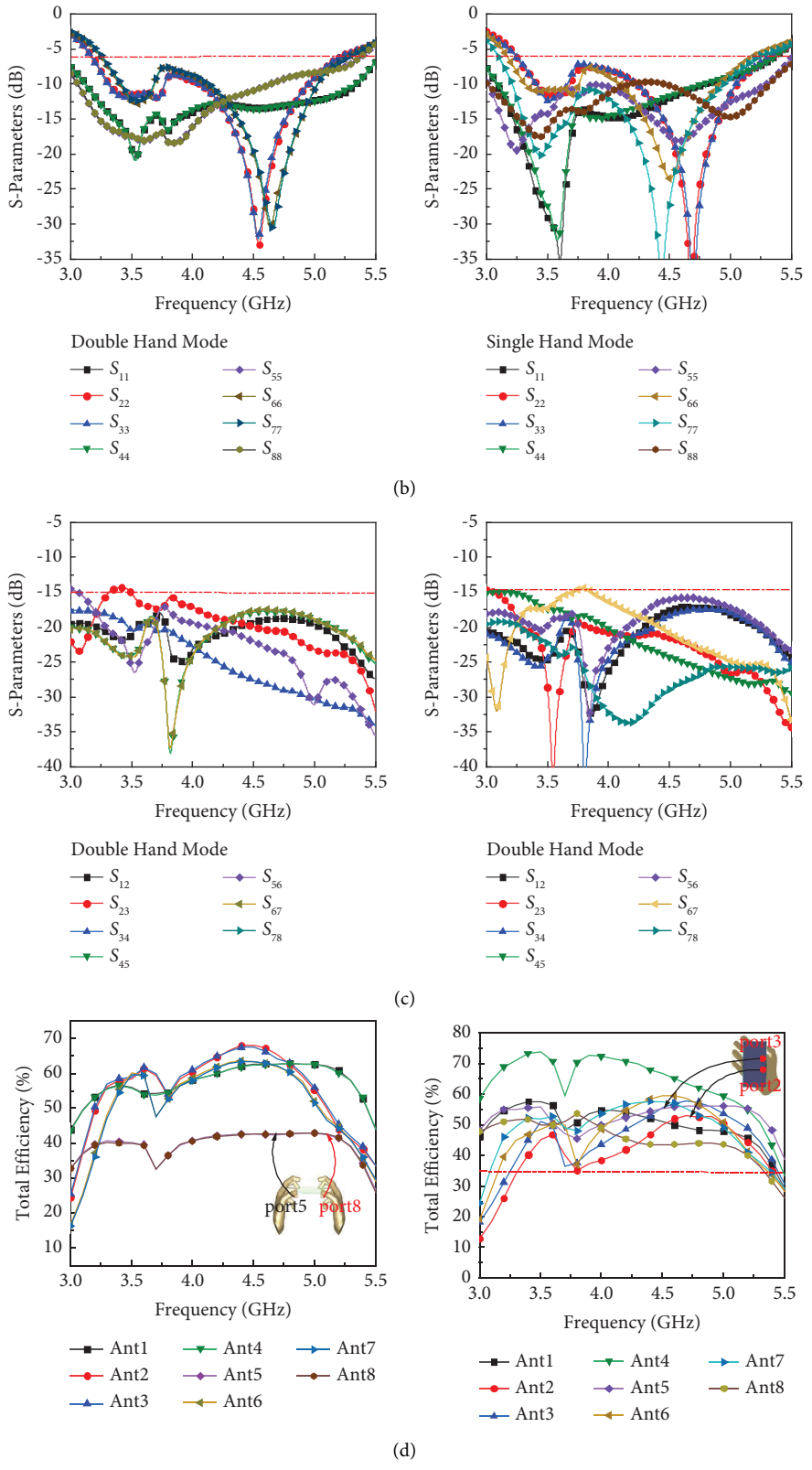

Figure 14: Two different representations of a handheld smartphone. (a) Dual-hand mode (DHM) and single-hand mode (SHM). (b) *S*-parameters of DHM and SHM. (c) Isolation degree of DHM and SHM. (d) Total efficiency of DHM and SHM.

4. Conclusions

In this article, a wideband 8 × 8 MIMO antenna system with desirable decoupling characteristics is designed for 5G terminal applications. First, the antenna element was designed as a combination of an open slot and two L-shaped folded monopoles. By adjusting the dimensions of the monopoles, the input impedance matching of antenna elements has been attained and the antenna element has realized a wide bandwidth. Afterward, the spatial arrangement of the antenna elements applicable to an 8 × 8 MIMO terminal antenna system is studied and determined. Due to the strong coupling between the adjacent ports, two types of decoupling methods have been designed. The T-shaped slot decoupling structure is designed between port1 and port2, and a quasi-M shaped slot structure with symmetric L-shaped parasitic strips is designed as multimode decoupling between port2 and port3. Since the system is symmetric, decoupling of the rest ports is duplicated readily. The proposed 8 × 8 antenna MIMO antenna system prototype is fabricated, simulated, and measured. The measured results show that all the antenna elements cover N77, N78, and N79 bands (3.28 to 5.05 GHz) and that the isolation degree between each port is higher than 14.5 dB. The measured envelope correlation coefficient between every two ports is less than 0.01. The proposed 8 × 8 MIMO wideband antenna system is undoubtedly suitable for sub-6 GHz terminal devices (e.g., ultra-thin smartphones) with wide frequency coverage and low port correlation.

Data Availability

The data that support the findings of this study are available from the corresponding author upon reasonable request.

Conflicts of Interest

The authors declare that they have no conflicts of interest.

Acknowledgments

This work was supported by the Natural Science Foundation of Fujian Province (2021J05178), the Natural Science Foundation of Xiamen (3502Z20227209), the Ktp project (202135040138), the Youth Top Talent Program of Jimei University (ZR2019001), and the Scientific Research Foundation of Jimei University (ZQ2021001).

References

[1] C.-Y.-D. Sim, H.-Y. Liu, and C.-J. Huang, "Wideband MIMO antenna array design for future mobile devices operating in the 5G NR frequency bands n77/n78/n79 and LTE band 46," *IEEE Antennas and Wireless Propagation Letters*, vol. 19, no. 1, pp. 74–78, 2020.

[2] A. Zhao and Z. Ren, "Wideband MIMO antenna systems based on coupled-loop antenna for 5G N77/N78/N79 applications in mobile terminals," *IEEE Access*, vol. 7, pp. 93761–93771, 2019.

[3] Z. Ren, A. Zhao, and S. Wu, "MIMO antenna with compact decoupled antenna pairs for 5G mobile terminals," *IEEE Antennas and Wireless Propagation Letters*, vol. 18, no. 7, pp. 1367–1371, 2019.

[4] K.-L. Wong, M.-F. Jian, and W.-Y. Li, "Low-profile wideband four-corner-fed square patch antenna for 5G MIMO mobile antenna application," *IEEE Antennas and Wireless Propagation Letters*, vol. 20, no. 12, pp. 2554–2558, 2021.

[5] A. Zhao and Z. Ren, "Size reduction of self-isolated MIMO antenna system for 5G mobile phone applications," *IEEE Antennas and Wireless Propagation Letters*, vol. 18, no. 1, pp. 152–156, 2019.

[6] Y. Ye, X. Zhao, and J. Wang, "Compact high-isolated MIMO antenna module with chip capacitive decoupler for 5G mobile terminals," *IEEE Antennas and Wireless Propagation Letters*, vol. 21, no. 5, pp. 928–932, 2022.

[7] D. R. Kumar, G. V. Babu, K. S. Narayan, and N. Raju, "Investigation of 10-port coupled fed slotted MIMO antenna system for 5G mobile handset," *International Journal of Microwave and Wireless Technologies*, vol. 14, no. 7, pp. 892–905, 2021.

[8] J. Li, X. Zhang, Z. Wang et al., "Dual-band eight-antenna array design for MIMO applications in 5G mobile terminals," *IEEE Access*, vol. 7, pp. 71636–71644, 2019.

[9] A. Zhao, Z. Ren, and S. Wu, "Broadband MIMO antenna system for 5G operations in mobile phones," *International Journal of RF and Microwave Computer-Aided Engineering*, vol. 29, no. 10, Article ID e21857, 2019.

[10] L. Cui, J. Guo, Y. Liu, and C.-Y.-D. Sim, "An 8-element dual-band MIMO antenna with decoupling stub for 5G smartphone applications," *IEEE Antennas and Wireless Propagation Letters*, vol. 18, no. 10, pp. 2095–2099, 2019.

[11] M. Abdullah, S. H. Kiani, and A. Iqbal, "Eight element multiple-input multiple-output (MIMO) antenna for 5G mobile applications," *IEEE Access*, vol. 7, pp. 134488–134495, 2019.

[12] S. H. Kiani, A. Iqbal, S.-W. Wong, H. S. Savci, M. Alibakhshikenari, and M. Dalarsson, "Multiple elements MIMO antenna system with broadband operation for 5th generation smart phones," *IEEE Access*, vol. 10, pp. 38446–38457, 2022.

[13] S. H. Kiani, M. Marey, H. Ş. Savci et al., "Dual-band multiple-element MIMO antenna system for next-generation smartphones," *Applied Sciences*, vol. 12, no. 19, 2022.

[14] S. H. Kiani, M. Khan, U. Rafique et al., "High performance eight-port dual-band MIMO antenna system for 5G devices," *Micromachines*, vol. 13, no. 6, 2022.

[15] C. Zhang, Z. Chen, X. Shi et al., "A dual-band eight-element MIMO antenna array for future ultrathin mobile terminals," *Micromachines*, vol. 13, no. 8, 2022.

[16] A. Ullah, N. Ojaroudi Parchin, A. S. Amar, and R. A. Abd-Alhameed, "Eight-element antenna array with improved radiation performances for 5G hand-portable devices," *Electronics*, vol. 11, no. 18, 2022.

[17] L. Chang and H. Wang, "Miniaturized wideband four-antenna module based on dual-mode PIFA for 5G 4 × 4 MIMO applications," *IEEE Transactions on Antennas and Propagation*, vol. 69, no. 9, pp. 5297–5304, 2021.

[18] Y. Hei, J. He, and W. Li, "Wideband decoupled 8-element MIMO antenna for 5G mobile terminal applications," *IEEE Antennas and Wireless Propagation Letters*, vol. 20, no. 8, pp. 1448–1452, 2021.

[19] L. Sun, Y. Li, and Z. Zhang, "Wideband integrated quad-element MIMO antennas based on complementary antenna pairs for 5G smartphones," *IEEE Transactions on Antennas and Propagation*, vol. 69, no. 8, pp. 4466–4474, 2021.

[20] L. Sun, Y. Li, Z. Zhang, and Z. Feng, "Wideband 5G MIMO antenna with integrated orthogonal-mode dual-antenna pairs for metal-rimmed smartphones," *IEEE Transactions on Antennas and Propagation*, vol. 68, no. 4, pp. 2494–2503, 2020.

[21] X.-T. Yuan, Z. Chen, T. Gu, and T. Yuan, "A wideband PIFA-pair-based MIMO antenna for 5G smartphones," *IEEE Antennas and Wireless Propagation Letters*, vol. 20, no. 3, pp. 371–375, 2021.

[22] X.-T. Yuan, W. He, K.-D. Hong, C.-Z. Han, Z. Chen, and T. Yuan, "Ultra-wideband MIMO antenna system with high element-isolation for 5G smartphone application," *IEEE Access*, vol. 8, pp. 56281–56289, 2020.

[23] U. Rafique, S. Khan, M. M. Ahmed et al., "Uni-planar MIMO antenna for sub-6 GHz 5G mobile phone applications," *Applied Sciences*, vol. 12, no. 8, 2022.

[24] S. H. Kiani, A. Altaf, M. R. Anjum et al., "MIMO antenna system for modern 5G handheld devices with healthcare and high rate delivery," *Sensors*, vol. 21, no. 21, 2021.

[25] M. N. Zahid, Z. Gaofeng, S. H. Kiani et al., "H-shaped eight-element dual-band MIMO antenna for sub-6 GHz 5G smartphone applications," *IEEE Access*, vol. 10, pp. 85619–85629, 2022.

[26] L. Sun, H. Feng, Y. Li, and Z. Zhang, "Compact 5G MIMO mobile phone antennas with tightly arranged orthogonal-mode pairs," *IEEE Transactions on Antennas and Propagation*, vol. 66, no. 11, pp. 6364–6369, 2018.

[27] Y. Wang and Z. Du, "A wideband printed dual-antenna system with a novel neutralization line for mobile terminals," *IEEE Antennas and Wireless Propagation Letters*, vol. 12, pp. 1428–1431, 2013.

[28] A. C. K. Mak, C. R. Rowell, and R. D. Murch, "Isolation enhancement between two closely packed antennas," *IEEE Transactions on Antennas and Propagation*, vol. 56, no. 11, pp. 3411–3419, 2008.

[29] L. Sun, Y. Li, Z. Zhang, and H. Wang, "Self-decoupled MIMO antenna pair with shared radiator for 5G smartphones," *IEEE Transactions on Antennas and Propagation*, vol. 68, no. 5, pp. 3423–3432, 2020.

[30] L. Sun, Y. Li, and Z. Zhang, "Wideband decoupling of integrated slot antenna pairs for 5G smartphones," *IEEE Transactions on Antennas and Propagation*, vol. 69, no. 4, pp. 2386–2391, 2021.

[31] H. Xu, H. Zhou, S. Gao, H. Wang, and Y. Cheng, "Multimode decoupling technique with independent tuning characteristic for mobile terminals," *IEEE Transactions on Antennas and Propagation*, vol. 65, no. 12, pp. 6739–6751, 2017.

[32] M. Alibakhshikenari, B. S. Virdee, P. Shukla et al., "Isolation enhancement of densely packed array antennas with periodic MTM-photonic bandgap for SAR and MIMO systems," *IET Microwaves, Antennas and Propagation*, vol. 14, no. 3, pp. 183–188, 2020.

[33] T. Roshna, U. Deepak, V. Sajitha, K. Vasudevan, and P. Mohanan, "A compact UWB MIMO antenna with reflector to enhance isolation," *IEEE Transactions on Antennas and Propagation*, vol. 63, no. 4, pp. 1873–1877, 2015.

[34] G. Zhai, Z. N. Chen, and X. Qing, "Enhanced isolation of A closely spaced four-element MIMO antenna system using metamaterial mushroom," *IEEE Transactions on Antennas and Propagation*, vol. 63, no. 8, pp. 3362–3370, 2015.

[35] M. Alibakhshikenari, B. S. Virdee, C. H. See, R. A. Abd-Alhameed, F. Falcone, and E. Limiti, "Surface wave reduction in antenna arrays using metasurface inclusion for MIMO and SAR systems," *Radio Science*, vol. 54, no. 11, pp. 1067–1075, 2019.

[36] M. Alibakhshikenari, C. H. See, B. Virdee, and R. A. Abd-Alhameed, "Meta-surface wall suppression of mutual coupling between microstrip patch antenna arrays for THz-band applications," *Progress In Electromagnetics Research Letters*, vol. 75, 2018.

[37] M. Alibakhshikenari, M. Khalily, B. S. Virdee, C. H. See, R. A. Abd-Alhameed, and E. Limiti, "Mutual-coupling isolation using embedded metamaterial EM bandgap decoupling slab for densely packed array antennas," *IEEE Access*, vol. 7, pp. 51827–51840, 2019.

[38] M. Alibakhshikenari, B. S. Virdee, C. H. See et al., "Study on isolation improvement between closely-packed patch antenna arrays based on fractal metamaterial electromagnetic bandgap structures," *IET Microwaves, Antennas and Propagation*, vol. 12, no. 14, pp. 2241–2247, 2018.

[39] H. Zhou, D. Wu, M. Zhu, Y. Qiu, G. Yu, and H. M. Zhou, "Wideband low-profile 8 × 8 MIMO antenna based IFA pair for ultrathin 5G smartphones," *International Journal of Antennas and Propagation*, vol. 2022, Article ID 5281470, 10 pages, 2022.

[40] D. Wu, Y. Qiu, G. Yu et al., "Decoupling technique using ferrite-film loading for 5G MIMO applications," *International Journal of Antennas and Propagation*, vol. 2022, Article ID 2028146, 12 pages, 2022.

[41] W.-C. Jhang, J.-S. Sun, and G. Oliveri, "Small antenna design of triple band for WIFI 6E and WLAN applications in the narrow border laptop computer," *International Journal of Antennas and Propagation*, vol. 2021, Article ID 7334206, 8 pages, 2021.

[42] Y. Li, C.-Y.-D. Sim, Y. Luo, and G. Yang, "High-isolation 3.5 GHz eight-antenna MIMO array using balanced open-slot antenna element for 5G smartphones," *IEEE Transactions on Antennas and Propagation*, vol. 67, no. 6, pp. 3820–3830, 2019.

[43] V. Thakur, N. Jaglan, and S. D. Gupta, "Side edge printed eight-element compact MIMO antenna array for 5G smartphone applications," *Journal of Electromagnetic Waves and Applications*, vol. 36, no. 12, pp. 1685–1701, 2022.

[44] N. Jaglan, S. D. Gupta, B. K. Kanaujia, and M. S. Sharawi, "10 element sub-6-GHz multi-band double-T based MIMO antenna system for 5G smartphones," *IEEE Access*, vol. 9, pp. 118662–118672, 2021.

[45] N. Jaglan, S. D. Gupta, and M. S. Sharawi, "18 element massive MIMO/diversity 5G smartphones antenna design for sub-6 GHz LTE bands 42/43 applications," *IEEE Open Journal of Antennas and Propagation*, vol. 2, pp. 533–545, 2021.